Available online at www.sciencedirect.com
ScienceDirect
Trans. Nonferrous Met. Soc. China 30(2020) 765−773
Transactions of Nonferrous Metals Society of China
www.tnmsc.cn

Effect of calcination temperature on microstructure and photocatalytic activity of BiOX (X=Cl, Br)

Si-mei FU[1], Gang-sen LI[1], Xing WEN[1], Cai-mei FAN[1], Jian-xin LIU[1], Xiao-chao ZHANG[1], Rui LI[1,2]

1. College of Chemistry and Chemical Engineering, Taiyuan University of Technology, Taiyuan 030024, China;
2. Shenzhen Batian Ecological Engineering Co., Ltd., Shenzhen 518057, China

Received 20 May 2019; accepted 5 January 2020

Abstract: A series of BiOX (X=Cl, Br) were prepared by simple hydrolysis and then calcined at various temperatures and they were characterized by XRD, Raman, SEM, DSC−TGA, BET and UV−Vis. The photocatalytic activity was evaluated by photocatalytic degradation of methyl orange (MO) solution under simulated solar light irradiation. The results show that the phase structure, crystallite size, morphology, specific surface area, porous structure, and the absorption band-edges are related to the calcination temperature. For BiOBr, it has completely transformed to $Bi_{24}O_{31}Br_{10}$ at 600 °C and begins to transform to Bi_2O_3 at 800 °C. As for BiOCl, it begins to transform to $Bi_{24}O_{31}Cl_{10}$ at 600 °C and completely transforms to $Bi_{24}O_{31}Cl_{10}$ at 800 °C. Finally, the photocatalytic activity of BiOCl decreases with the temperature increasing owing to decrease of the specific surface areas and pore size, while the photocatalytic activity of BiOBr increases in the first stage and then decreases, which is related to good crystallization and three-dimensional structure.

Key words: calcination; BiOX (X=Cl, Br) photocatalyst; microstructure; photocatalytic activity

1 Introduction

Energy and environmental resources are issues of increasing concern in modern society. Heterogeneous photocatalysis through semiconductor systems, as an environmental-friendly technology, has been considered to be a competitive and promising technology for environmental remediation and solar energy conversion [1−3]. Various semiconductor materials have been successfully synthesized as photocatalysts for pollutants removal from air or water, CO_2 capture, hydrogen generation, nitrogen fixation, organic synthesis, and selective oxidation of alcohol etc [4,5].

For a successful photocatalytic technology, an efficient semiconductor material is a crucial component. In recent years, BiOX (X=Cl, Br) has attracted massive research interest due to its unique layered-structure, indirect transition mode, suitable band-structure, high chemical and optical inertness, nontoxicity, cost effectiveness, and high corrosion resistance [6−8]. However, before putting the bismuth oxyhalides into practical application, some issues need to be addressed because the physical and chemical properties of BiOX (X=Cl, Br) all could have great influence on the photocatalytic performance [9,10]. Therefore, regulation of its physicochemical properties, which are considerably associated with the preparing methods and post-treatment condition, has become an important

Foundation item: Projects (21676178, 21506144, 21706179) supported by the National Natural Science Foundation of China; Project (2019L0138) supported by the Science and Technology Innovation Program of Higher Education Institutions in Shanxi Province, China; Project (201901D211100) supported by the Natural Science Foundation of Shanxi Province for Young Scientists, China

Corresponding author: Si-mei FU, Tel: +86-351-6018193, +86-351-6010182, E-mail: 28184931@qq.com;
Rui LI, E-mail: lirui13233699182@163.com

DOI: 10.1016/S1003-6326(20)65252-9

strategy for fine-tuning the photocatalytic activity. As one of the control parameters, the calcination temperature has become an important strategy for fine-tuning the physicochemical properties [11,12]. For instance, ZHANG et al [13] demonstrated that calcination is an effective treatment to increase the photoactivity of nanosized TiO_2 photocatalysts resulting from the improvement of crystallinity. YU et al [12] also observed that TiO_2 at 600 °C shows the highest photocatalytic activity owing to the largest formation rate of hydroxyl radicals and photocurrent. LIU et al [14] reported the preparation of $Bi_{24}O_{31}Cl_{10}$/BiOCl heterojunction via a simple thermal annealing method (up to 600 °C), which displays excellent photocatalytic efficiency and selectivity toward the conversion of benzyl alcohol to benzaldehyde under visible light irradiation.

Above studies show that calcination temperature has an influence on the crystalline phases, morphology and photocatalytic efficiency of photocatalysts. To date, there have been few researches to explore the effect of calcination temperature on the physical and chemical properties of BiOX (X=Cl, Br) [15,16]. BiOX (X=Cl, Br) photocatalysts are obtained via solvothermal approach, and alcohol solvents are used [16]. However, from a practical perspective, water should be the best solvent and hydrolysis should be the most environment-friendly and energy-saving synthetic method for BiOBr photocatalyst. Furthermore, the preparation methods and the reaction medium can also affect the original properties of BiOBr [17]. So, before putting the bismuth oxyhalides, which is prepared by hydrolysis method, into practical application, the effect of calcination temperature on BiOX (X=Cl, Br) prepared by simple hydrolysis method in water needs to be clarified and further investigated.

Here, we firstly prepared a series of BiOX (X=Cl, Br) photocatalysts by a simple hydrolysis method in water, and then explore the effect of calcination temperature on the physical and chemical properties of BiOX (X=Cl, Br). The as-prepared samples were characterized by XRD, Raman, SEM, TGA−TSC, BET and UV−vis diffuse reflectance spectra. The efficiency of photocatalytic activity using these prepared samples was evaluated on the basis of the photodegradation rate of MO in aqueous solution.

2 Experimental

2.1 Materials

Bismuth halide (BiX_3, X=Cl, Br), absolute ethanol and methyl orange were purchased from Alfa Aesar (Tianjin) Chemical Co. Ltd. and Tianjin Guangfu Technoligy Development Company Limited. The purities of the bismuth halide (BiX_3, X=Cl, Br) and the methyl orange are 99%, and they were used as received without further purification.

2.2 Preparation of photocatalysts

The BiOX (X=Cl, Br) were synthesized by a simple hydrolysis method. In a typical procedure, 0.5000 g of BiX_3 (X=Cl, Br) was initially dissolved in 15 mL deionized water at room temperature with continuous stirring. After stirring for 1 h, the mixture was filtered and washed with distilled water and absolute ethanol for several times, and then dried at 60 °C for 5 h. Finally, in order to explore the effect of calcination temperature on the physical and chemical properties of BiOX (X=Cl, Br), the samples were calcined at different temperatures in air for 2 h. The resulting samples were denoted as BOX-*n*, where *n* (0, 2, 4, 6 and 8) represents different temperatures (room temperature, 200, 400, 600 and 800 °C).

2.3 Sample characterization

The crystalline phases of as-prepared samples were examined by a Rigaku D/MAX−2500 diffractometer with monochromatized Cu K_α radiation (λ=0.15406 nm) within the 2θ range from 10° to 80°. The operation voltage and current were 40 kV and 30 mA, respectively, and the scanning speed was set as 8 (°)/min. The microstructures of samples were recorded on a Nanosem 430 field emission scanning electron microscope at an operating voltage of 10 kV. The Brunauer−Emmett−Teller (BET) surface areas were measured by nitrogen adsorption isotherm measurements at 77 K on a JW−BK instrument. Ultraviolet-visible diffused reflectance spectra of the samples were obtained for the dry-pressed film samples. The differential scanning colorimetry/thermogravimetric analyses (DSC−TGA) were carried out on a Henven−1 comprehensive thermal analyzer (made in China) with a heating program at 10 °C/min from 30 to 900 °C in air. Raman spectra were recorded

on the Horiba Jobin Yvon LabRAMHR800 instrument with the laser excitation of 514 nm.

2.4 Photocatalytic activity test

The photocatalytic activity experiments of the products for the degradation of methyl orange (MO, 99%) were performed at ambient temperature using a 350 W xenon lamp as the simulated solar light source. The distance between the light and the center of the reactor was 20 cm. Typically, 100 mg of photocatalyst was dispersed in 100 mL of 10 mg/L MO aqueous solution in a container. Then, the suspension was continuously stirred in the dark to achieve the adsorption–desorption equilibrium prior to visible light irradiation. During the degradation, the MO solution was taken out at given time intervals and monitored by colorimetry with a Varian Cary−50 UV−Vis spectrophotometer. The degradation efficiency (D) of MO was calculated by

$$D=\left(1-c_t/c_0\right)\times 100\% \quad (1)$$

where c_0 and c_t are the initial concentration of MO and the concentration of MO after irradiation for a period of t, respectively, and the detection wavelength of the MO is 464 nm.

3 Results and discussion

3.1 Structure and morphology analysis

The phase structure and crystallite sizes of the BiOX (X=Cl, Br) samples calcined at different temperatures were evidenced by X-ray diffraction (XRD) characterization. As shown in Fig. 1(a), all the diffraction peaks of BiOCl at room temperature, 200 and 400 °C correspond well to pure BiOCl with space group *P*4/*nmm* (JCPDS No. 06−249). Furthermore, with the increase of calcination temperatures (from room temperature to 400 °C), XRD peak intensities gradually increase and the width of XRD diffraction peaks becomes narrow, which indicates an improvement in the crystallinity for the BiOCl [16]. However, when the calcination temperature is increased to 600 °C, the new diffraction peak at 2θ of 30.03° appears and the characteristic diffraction peaks for BiOCl remain. The new reflection peaks are ascribed to $Bi_{24}O_{31}Cl_{10}$ (JCPDS No. 70-4761). At 800 °C, BiOCl totally

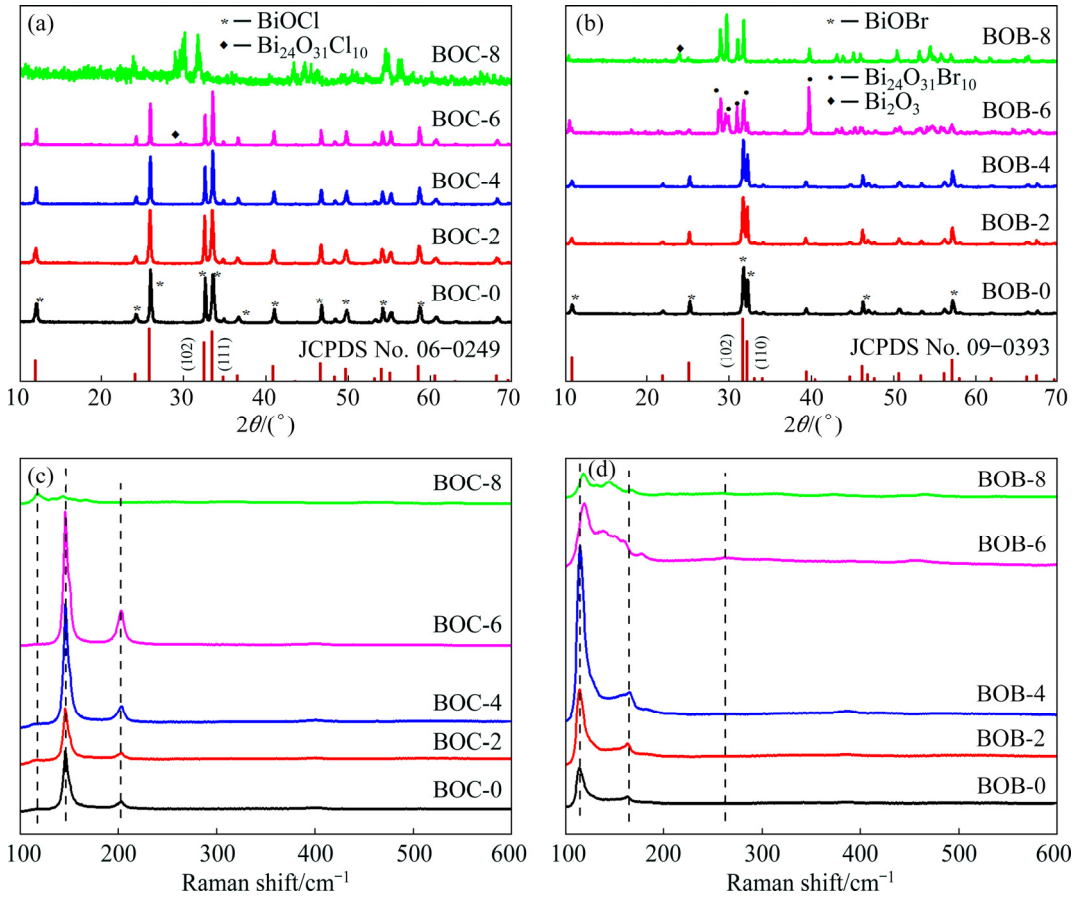

Fig. 1 XRD patterns (a, b) and Raman spectra (c, d) of as-prepared BiOX samples at different calcination temperatures

changes to $Bi_{24}O_{31}Cl_{10}$. For BiOBr (Fig. 1(b)), it is observed that when the calcination temperature is below 400 °C, the XRD patterns correspond well to the tetragonal BiOBr structure with the space group of *P*4/*nmm* (JCPDS No. 09−0393). Similar with BiOCl, when the calcination temperature varies from room temperature to 400 °C, the crystallization of BiOBr is enhanced. In the temperature range from 400 to 600 °C, the (102) and (110) diffraction peaks of BiOBr disappear and the new reflection peaks at 2θ of 29.11, 29.87, 31.15 and 39.91° appear, which is attributed to $Bi_{24}O_{31}Br_{10}$. Finally, BiOBr totally changes to $Bi_{24}O_{31}Br_{10}$ at 800 °C. At the same time, small peak of Bi_2O_3 is observed. XRD results show that the calcination temperature is of great importance for the crystallization and phase structures.

The Raman spectra (Figs. 1(c) and (d)) are presented to further confirm the structure of BiOX (X=Cl, Br) crystals. For BiOX (X=Cl, Br) with a tetragonal structure of space group *P*4/*nnm*, the Raman active modes are A_{1g}, B_{1g} and E_g. BiOCl at different calcination temperatures has two distinguishable bands at 146 and 200 cm^{-1}, assigned to the A_{1g} and E_g internal Bi—Cl stretching mode, respectively [14,18]. With increasing the calcination temperature to 800 °C, there is a new band located at 118 cm^{-1} close to that of pure $Bi_{24}O_{31}Cl_{10}$, indicating the presence of $Bi_{24}O_{31}Cl_{10}$ [14]. The band of $Bi_{24}O_{31}Cl_{10}$ is not obtained at 600 °C, which is due to the low content of $Bi_{24}O_{31}Cl_{10}$. Furthermore, as for BiOBr (Fig. 1(d)), it is noticed that the strong band at 113 and 165 cm^{-1} can be assigned to A_{1g} and E_g internal Bi—Br stretching mode [19]. At 600 and 800 °C, the new bands at 150 and 263 cm^{-1} appear, indicating the presence of $Bi_{24}O_{31}Br_{10}$ [20]. The band of Bi_2O_3 is not obtained at 800 °C, which is also due to the low content of Bi_2O_3. This indicates a good agreement with the results of XRD. In addition, the average primary crystal sizes of BOC-0, BOC-2, BOC-4, BOC-6 and BOC-8 are 337 nm, 358 nm, 383 nm, 850 nm and 1.489 μm, respectively. The average primary crystal sizes of BOB-0, BOB-2, BOB-4, BOB-6 and BOB-8 are 267, 315, 387, 467 and 562 nm, respectively, from the XRD data.

The morphologies of BiOX (X=Cl, Br) at various calcination temperatures observed with scanning electronic microscope (SEM) are shown in Fig. 2 and Fig. 3, respectively. As illustrated in Fig. 2(a), the BiOCl without calcination is composed of a large quantity of small flakes. When BiOCl is calcined at 200 °C (Fig. 2(b)), the produced sample has a similar sheet-shaped structure while the crystallite size becomes larger. With further increase in calcination temperature, the flakes gradually disappear and much bigger plate-like particles appear at 400 and 600 °C (Figs. 2(c, d)). BiOCl totally changes to $Bi_{24}O_{31}Cl_{10}$ at 800 °C with larger plate-like particles (Fig. 2(e)).

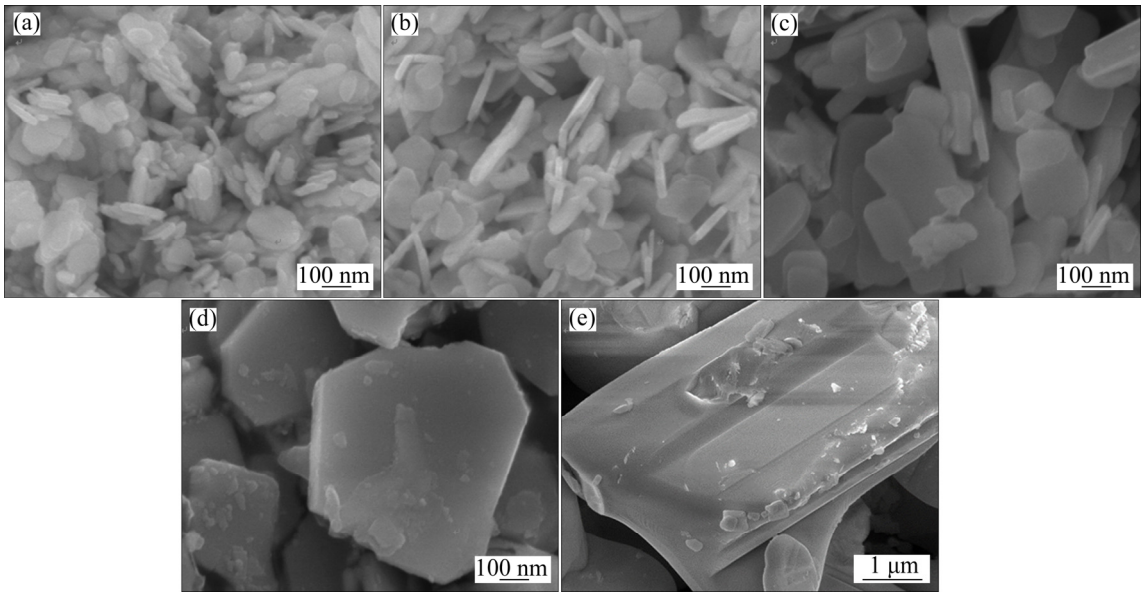

Fig. 2 SEM images of as-prepared BiOCl samples at different calcination temperatures: (a) No calcination; (b) 200 °C; (c) 400 °C; (d) 600 °C; (e) 800 °C

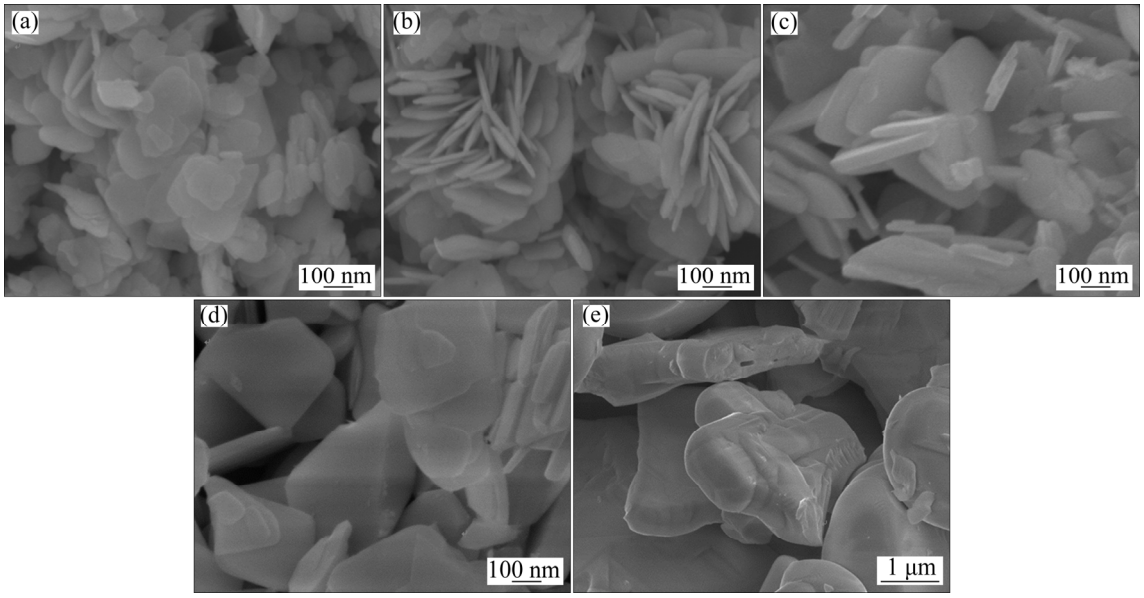

Fig. 3 SEM images of as-prepared BiOBr samples at different calcination temperatures: (a) No calcination; (b) 200 °C; (c) 400 °C; (d) 600 °C; (e) 800 °C

As for BiOBr, it can be seen that BiOBr without calcination is also composed of a large quantity of small flakes (Fig. 3(a)). However, with further increase in calcination temperature, the flakes congregate into flower-like microsphere morphology at 200 °C (Fig. 3(b)). The formation of three-dimensional microspheres not only can provide rich interface and lots of nano- and macro-pores on the BiOBr surface, but also is beneficial to the dye absorption and light absorption [21,22]. At 400 °C (Fig. 3(c)), as the calcination temperature increases, the flower-like microspheres are thinned. When BiOBr is calcined at 600 °C, the morphology of the produced sample changes and no flower-like particles is found, which is caused by the decomposition of BiOBr and the formation of $Bi_{24}O_{31}Br_{10}$ (Fig. 3(d)). Surprisingly, at 800 °C, the bigger block is noticed (Fig. 3(e)).

3.2 DSC and TGA analysis

The thermal stability of BiOX (X=Cl, Br) were analyzed by DSC−TGA. As for BiOCl (Fig. 4(a)), it can be seen that BiOCl has no significant mass loss from 30 to 700 °C, while it starts to sharply decompose at 700 °C with a remarkable endothermic phenomenon, indicating the decomposition of BiOCl. The total mass loss of BiOCl is around 23.50%. By careful observation, there are two exothermic peaks on the DSC curve of BiOCl: one peak appears in the range of 30 and 300 °C, which is caused by the evaporation of small water molecules, and the other appears at 800 °C, which may correspond to the transformation of BiOCl to $Bi_{24}O_{31}Cl_{10}$. For BiOBr (Fig. 4(b)), it can be found that the TGA curve of BiOBr obviously decreases at 600 and 700 °C, manifesting the decomposition of BiOBr. The total mass loss of BiOBr is around 17.48%. Furthermore, there are three exothermic peaks on the DSC curve of BiOBr. The exothermic phenomenon in the range between 30 and 300 °C is similar to that of BiOCl. The exothermic spiculate peak at 600 °C should correspond to the transformation of BiOBr to $Bi_{24}O_{31}Br_{10}$. The exothermic spiculate peak at 800 °C should correspond to the transformation of BiOBr to Bi_2O_3. The DSC−TGA results further indicate that BiOCl is more stable than BiOBr, and the transformation of BiOCl and BiOBr is consistent with XRD.

3.3 Surface areas analysis

The specific surface areas and porous structure of BiOX (X=Cl, Br) were investigated using nitrogen adsorption and desorption isotherms, and the results are shown in Fig. 5. All the isotherms correspond to a Type IV isotherm characteristic with H3 hysteresis loop, indicating the presence of

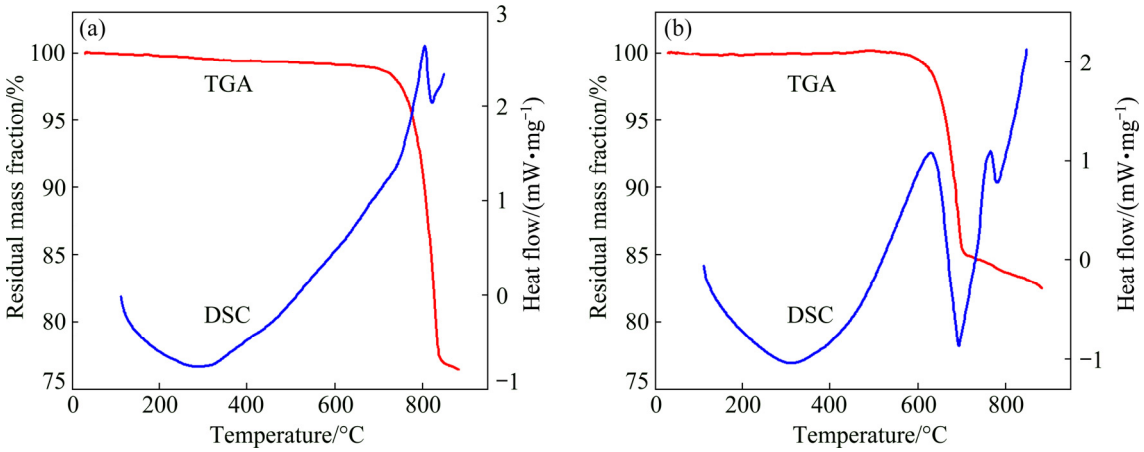

Fig. 4 DSC−TGA curves of as-prepared BiOCl (a) and BiOBr (b)

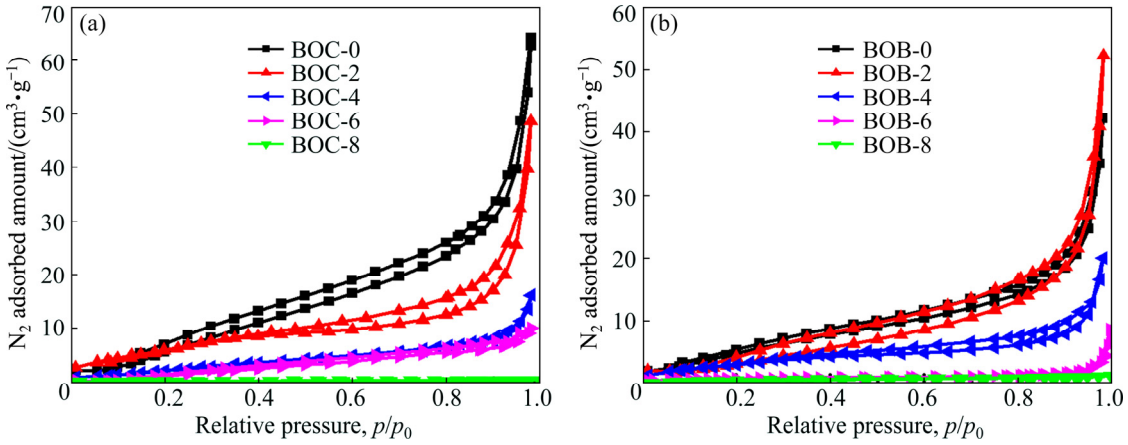

Fig. 5 Nitrogen adsorption–desorption isotherms of as-prepared BiOCl (a) and BiOBr (b) samples at different calcination temperatures

mesoporous structure [23]. In addition, the textural parameters of BiOX (X=Cl, Br) were concluded from the nitrogen adsorption−desorption isotherm and are shown in Fig. 5. It can be seen that the BET surface area and average pore size values of BiOCl decline with the increase of the calcination temperature. The BET surface area values of BiOBr decrease while pore size values of BiOBr rise in the first stage and then decrease with increasing the calcination temperature, which may be resulted from the change of morphology of BiOBr, agreeing with the observation of SEM [24]. Furthermore, the larger surface areas and pore structure both play an important role in enhancing photocatalytic activities for BiOBr sample [25].

3.4 UV−Vis diffuse reflectance spectra

The optical properties of BiOX (X=Cl, Br) were measured by UV−Vis DRS, as plotted in Fig. 6. It is obviously found that the absorption band-edges of BOC-0, 2, 4, 6, 8 are 366, 381, 382, 384 and 465 nm, respectively. The band gap (E_g) of BiOX (X=Cl, Br) follows the formula of E_g= 1239/λ_g [26], where λ_g is the bandgap wavelength. So, the optical band gaps of BiOCl are estimated to be about 3.38, 3.25, 3.24, 3.22 and 2.66 eV, respectively. As for BiOBr, the absorption band-edges of BOB-0, 2, 4, 6, 8 are 453, 460, 455, 450 and 464 nm and the estimated optical band gaps are 2.73, 2.69, 2.72, 2.75 and 2.67 eV, respectively.

3.5 Photocatalytic activity

MO is used as the probe molecule to evaluate the photocatalytic performances of the BiOX (X= Cl, Br) samples. Figure 7 shows the photocatalytic abilities of as-prepared samples to degrade MO under the simulated solar light source. During the photocatalytic reaction, the activity and degradation rate of BiOCl clearly decrease with the increase of calcination temperature from room temperature to

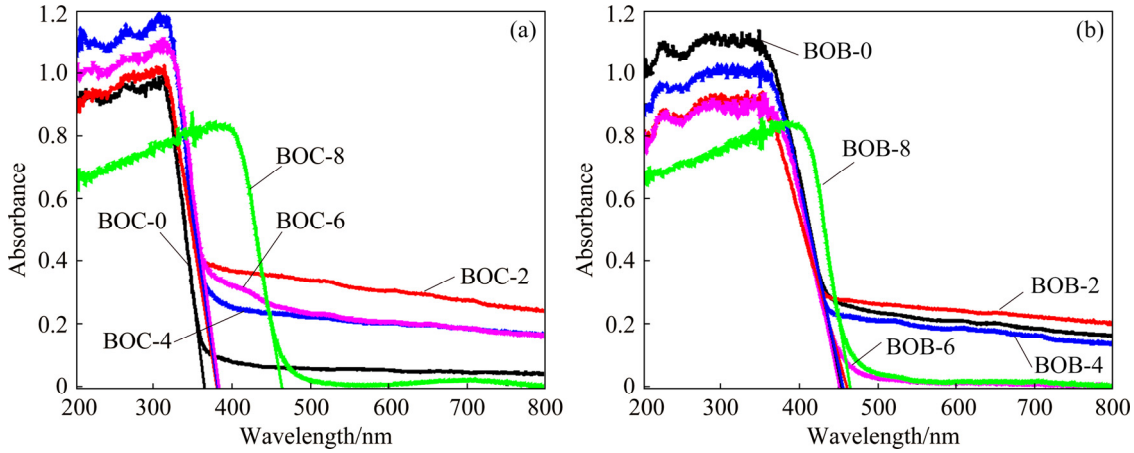

Fig. 6 UV−Vis absorption spectra of as-prepared BiOCl (a) and BiOBr (b) samples at different calcination temperatures

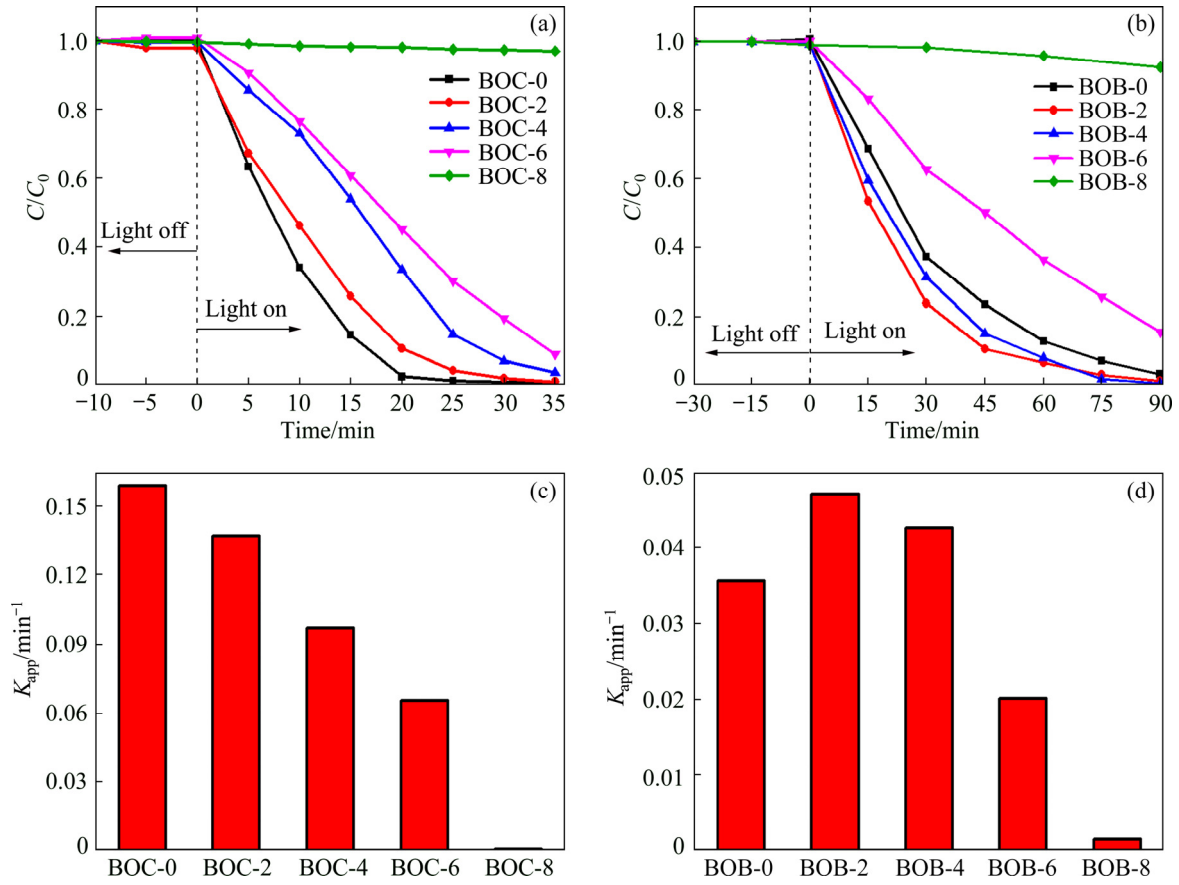

Fig. 7 Photocatalytic activities (a, b) and apparent rate constants (c, d) of as-prepared BiOCl (a, c) and BiOBr (b, d) samples at different calcination temperatures

600 °C (Fig. 7(a)). The apparent reaction rate constant (K_{app}) of BOC-0, BOC-2, BOC-4, BOC-6 and BOC-8 decreases from 0.1589 to 0.007 min^{-1}, which means that BOC-8 almost has no photocatalytic activity, implying that raising temperature can depress the photocatalytic activity. As for BiOBr, the removal efficiency of BOB-2 and BOB-4 is higher than that of BOB-0. It can also be concluded from Fig. 7(d) that the rate constants of BOB-2 and BOB-4 are 0.0471 and 0.0426 min^{-1}, respectively. With further increase in the calcination temperature, the photocatalytic activity declines and has little activity at 800 °C. The photocatalytic activity is also associated with parameters of the materials, including catalyst structure, size, crystallinity, specific surface areas and pore

structure [27]. Therefore, BOB-2 and BOB-4 exhibiting better photocatalytic activity than BOB-0 is ascribed to their flower-like microsphere morphology and pore structure, which can provide the lots of nano- and macro-pores on the surface and rich interface, inhibiting the recombination of photo-generated carriers and further leading to the increase of photocatalytic activity [28,29].

4 Conclusions

(1) A series of BiOX (X=Cl, Br) photocatalysts were prepared by a simple hydrolyzation method using $BiBr_3$ as precursor at room temperature in water and then calcined at various temperatures.

(2) For BiOBr, it has completely transformed to $Bi_{24}O_{31}Br_{10}$ at 600 °C and begins to transform to Bi_2O_3 at 800 °C. As for BiOCl, it begins to transform to $Bi_{24}O_{31}Cl_{10}$ at 600 °C and completely transforms to $Bi_{24}O_{31}Cl_{10}$ at 800 °C.

(3) Owing to decrease of the specific surface areas and pore size, the photocatalytic activity of BiOCl gradually declines. However, the photocatalytic activity of BiOBr rises in the first stage and then decreases, because of the good crystallization and three-dimensional structure.

References

[1] XU Yu-xia, LI Qing, XUE Huai-guo, PANG Huan. Metal-organic frameworks for direct electrochemical applications [J]. Coordination Chemistry Reviews, 2018, 376: 292−318.

[2] LIU Fu-yu, JIANG Yu-rou, CHEN Chiling-chang, LEE Wenlian-william. Novel synthesis of $PbBiO_2Cl$/BiOCl nanocomposite with enhanced visible-driven-light photocatalytic activity [J]. Catalysis Today, 2018, 300: 112−123.

[3] ZHAO Wen-hua, WEI Zhi-qiang, WU Xiao-juan, ZHANG Xu-dong, ZHANG Li, WANG Xuan. Microstructure and photocatalytic activity of Ni-doped ZnS nanorods prepared by hydrothermal method [J]. Transactions of Nonferrous Metals Society of China, 2019, 29: 157−164.

[4] MENG Nan-nan, REN Jian, LIU Yang, HUANG Yi, PETIT T, ZHANG Bin. Engineering oxygen-containing and amino groups into two-dimensional atomically-thin porous polymeric carbon nitrogen for enhanced photocatalytic hydrogen production [J]. Energy and Environmental Science, 2018, 11: 566−571.

[5] YUAN Ru-sheng, FAN Shao-long, ZHOU Hua-xi, DING Zheng-xin, LIN Sen, LI Zhao-hui, ZHANG Zi-zhong, XU Chao, WU Ling, WANG Xu-xu, FU Xian-zhi. Chlorine radical mediated photocatalytic activation of C—H bonds with visible light [J]. Angewandte Chemie International Edition, 2013, 52: 1035−1039.

[6] LI Rui, LIU Jian-xin, ZHANG Xiao-fang, WANG Ya-wen, WANG Yun-fang, ZHANG Chang-ming, ZHANG Xiao-chao, FAN Cai-mei, Iodide-modified $Bi_4O_5Br_2$ photocatalyst with tunable conduction band position for efficient visible-light decontamination of pollutants [J]. Chemical Engineering Journal, 2018, 339: 42−50.

[7] LIU Jian-xin, LI Rui, ZU Xiang, ZHANG Xiao-chao, WANG Yun-fang, WANG Ya-wen, FAN Cai-mei, Photocatalytic conversion of nitrogen to ammonia with water on triphase interfaces of hydrophilic-hydrophobic composite $Bi_4O_5Br_2$/ZIF-8 [J]. Chemical Engineering Journal, 2019, 371: 796−803.

[8] SHI Zhu-qing, WANG Yan, FAN Cai-mei, WANG Yun-fang, DING Guang-yue. Preparation and photocatalytic activity of BiOCl catalyst [J]. Transactions of Nonferrous Metals Society of China, 2011, 21: 2254−2258.

[9] YE Li-qun, JIN Xiao-li, LIU Chuan, DING Cheng-hua, XIE Hai-quan, CHU Ka-him, WONG Po-kung. Thickness-ultrathin and bismuth-rich strategies for BiOBr to enhance photoreduction of CO_2 into solar fuels [J]. Applied Catalysis B: Environmental, 2016, 187: 281−290.

[10] WU Dan, YE Li-qun, YIP Ho-yin, WONG Po-keungg. Organic-free synthesis of {001} facet dominated BiOBr nanosheets for selective photoreduction of CO_2 to CO [J]. Catalysis Science and Technology, 2017, 7: 265−271.

[11] GE Chen, HUANG Huai-yi, WANG Yi, ZHANG Ping-yu, ZHANG Qian-lin. Near-infrared luminescent osmium(II) complexes with an intrinsic rna-targeting capability for nucleolus imaging in living cells [J]. ACS Applied Bio Materials, 2018, 1: 1587−1593.

[12] YU Jia-guo, WANG Bo. Effect of calcination temperature on morphology and photoelectrochemical properties of anodized titanium dioxide nanotube arrays [J]. Applied Catalysis B: Environmental, 2010, 94: 295−302.

[13] ZHANG Qing-hong, GAO Lian, GUO Jing-kun. Effects of calcination on the photocatalytic properties of nanosized TiO_2 powders prepared by $TiCl_4$ hydrolysis [J]. Applied Catalysis B: Environmental, 2000, 26: 207−215.

[14] LIU Xiao-yan, SU Yi-guo, ZHAO Qing-hang, DU Chun-fang, LIU Zhi-liang. Constructing $Bi_{24}O_{31}Cl_{10}$/BiOCl heterojunction via a simple thermal annealing route for achieving enhanced photocatalytic activity and selectivity [J]. Scientific Reports, 2016, 6: 1−13.

[15] GU Shi-qing, WANG Lan, MAO Xin-you, YANG Li-ping, WANG Chuan-yi. Selective adsorption of Pb(II) from aqueous solution by triethylenetetramine-grafted polyacrylamide/vermiculite [J]. Materials, 2018, 11: 514−534.

[16] YU Chang-lin, ZHOU Wan-qin, YU Jimmcy, CAO Fang-fang, LI Xin. Thermal stability, microstructure and photocatalytic activity of the bismuth oxybromide photocatalyst [J]. Chinese Journal of Chemistry, 2012, 30: 721−726.

[17] LI Rui, Gao Xiao-ya, Fan Cai-mei, ZHANG Xiao-chao, WANG Ya-wen, WANG Yun-fang. A facile approach for the tunable fabrication of BiOBr photocatalysts with high activity and stability [J]. Applied Surface Science, 2015, 355: 1075−1082.

[18] WU Tian-li, LI Xiao-xia, ZHANG Ding-ke, DONG Fan,

CHEN Shi-jian. Efficient visible light photocatalytic oxidation of NO with hierarchical nanostructured 3D flower-like $BiOCl_xBr_{1-x}$ solid solutions [J]. Journal of Alloys and Compounds, 2016, 671: 318−327.

[19] ZHANG Da, LI Jing, WANG Qi-gang, WU Qing-sheng. High {001} facets dominated BiOBr lamellas: Facile hydrolysis preparation and selective visible-light photocatalytic activity [J]. Journal of Materials Chemistry A, 2013, 1: 8622−8629.

[20] LIANG Han-Pu, ZHANG Hui-min, HU Jin-song, GUO Yu-guo, WAN Li-jun, BAI Chun-li. Pt hollow nanospheres: Facile synthesis and enhanced electrocatalysts [J]. Angewandte Chemie International Edition, 2004, 43: 1540−1543.

[21] CHEN Lan, HUANG Rui, XIONG Miao, YUAN Qing, HE Jie, JIA Jing, YAO Meng-yuan, LUO Shen-lian, AU Chak-tong, YIN Shuang-fen. Room-temperature synthesis of flower-like BiOX (X=Cl, Br, I) hierarchical structures and their visible-light photocatalytic activity [J]. Inorganic Chemistry, 2013, 52: 11118−11125.

[22] FANG Wen, YU Chang-lin, LI Jia-de, ZHOU Wan-qin. Thermostability and photocatalytic performance of $BiOCl_{0.5}Br_{0.5}$ composite microspheres [J]. Journal of Materials Research, 2015, 30: 3125−3133.

[23] GARG S, YADAV M, CHANDRA A, HERNADI K. A Review on BiOX (X=Cl, Br and I) nano-/microstructures for their photocatalytic applications [J]. Journal of Nanoscience and Nanotechnology, 2019, 19: 280−294.

[24] ZHANG Li, YAN Jian-hui, ZHOU Min-jie, YU Yan-ping, LIU Ye, LIU You-nian. Photocatalytic degradation and inactivation of *Escherichia coli* by $ZnO/ZnAl_2O_4$ with heteronanostructures [J]. Transactions of Nonferrous Metals Society of China, 2014, 24: 743−749.

[25] CHENG Li-jun, YAN Jian-cheng, ZHAO Shi-zong, HAO Liang. Multiple charge carrier transfer pathways in $BiOBr/Bi_2O_3/BiO_{0.67}F_{1.66}$ ternary composite with high adsorption and photocatalytic performance [J]. Journal of Alloys and Compounds, 2019, 778: 924−932.

[26] LIU Jian-xin, LI Rui, HU Ying-yuan, LI Tan, JIA Ze-hui, WANG Yun-fang, WANG Ya-wen, ZHANG Xiao-chao, FAN Cai-mei, Harnessing Ag nanofilm as an electrons transfer mediator for enhanced visible light photocatalytic performance of Ag@AgCl/Ag nanofilm/ZIF-8 photocatalyst [J]. Applied Catalysis B: Environmental, 2017, 202: 64−71.

[27] JIANG Jing, ZHAO Kun, XIAO Xia-yi, ZHANG Li-zhi. Synthesis and facet-dependent photoreactivity of BiOCl single-crystalline nanosheets [J]. Journal of the American Chemical Society, 2012, 134: 4473−4476.

[28] YU Jia-guo, MA Ting-ting, LIU Sheng-wei. Enhanced photocatalytic activity of mesoporous TiO_2 aggregates by embedding carbon nanotubes as electron-transfer channel [J]. Physical Chemistry Chemical Physics, 2011, 13: 3491−3501.

[29] MENG Yan, Preparation of $Y_2Cu_2O_5$ photocatalyst for H_2 production under simulated sunlight irradiation [J]. Transactions of Nonferrous Metals Society of China, 2012, 22: 184−189.

煅烧温度对 BiOX(X=Cl, Br)的微观结构和光催化活性的影响

付思美[1]，李刚森[1]，温 幸[1]，樊彩梅[1]，刘建新[1]，张小超[1]，李 瑞[1,2]

1. 太原理工大学 化学化工学院，太原 030024；
2. 深圳市芭田生态工程股份有限公司，深圳 518057

摘 要：采用简单水解法和后热处理制备一系列 BiOX(X=Cl, Br)光催化剂，通过 XRD、拉曼、SEM、DSC−TGA、BET 和 UV−Vis 表征所获得的样品，并且通过在模拟太阳光源下光催化降解甲基橙(MO)来评价煅烧温度对样品活性的影响。结果表明，催化剂的相结构、晶粒尺寸、形貌、比表面积、多孔结构和吸收带边缘均与焙烧温度有关。BiOBr 在 600 °C 已完全转变为 $Bi_{24}O_{31}Br_{10}$，并在 800 °C 开始转变为 Bi_2O_3；而 BiOCl 在 600 °C 才开始转变为 $Bi_{24}O_{31}Cl_{10}$，在 800 °C 全部转化为 $Bi_{24}O_{31}Cl_{10}$。BiOCl 的光催化活性随温度的升高而降低，这归因于比表面积和孔径的减小；而 BiOBr 的光催化活性先升高后降低，这与其良好的结晶和三维结构有关。

关键词：焙烧；BiOX(X=Cl, Br)光催化剂；微观结构；光催化活性

(Edited by Bing YANG)